MOLECULAR AND CELLULAR BIOLOGY, Jan. 2009, p. 150–156 Vol. 29, No. 1
0270-7306/09/$08.00+0 doi:10.1128/MCB.00997-08

Weak but Uniform Enrichment of the Histone Variant macroH2A1 along the Inactive X Chromosome▽

Flore Mietton,[1] Aditya K. Sengupta,[2] Annie Molla,[1] Gisele Picchi,[4] Sophie Barral,[1] Laurent Heliot,[3] Thierry Grange,[4] Anton Wutz,[2] and Stefan Dimitrov[1]*

Institut Albert Bonniot, INSERM/UJF-U823, Site Santé-BP 170, 38042 Grenoble Cedex 9, France[1]; Research Institute of Molecular Pathology, Dr. Bohr-Gasse 7, A-1030 Vienna, Austria[2]; Institut de Recherche Interdisciplinaire, FRE 2963 CNRS/Université de Lille I/Université de Lille II, Lille, France[3]; and Institut Jacques Monod, CNRS, Universités Paris 6 et 7, Tour 43, 2 Place Jussieu, 75251 Paris Cedex 06, France[4]

Received 24 June 2008/Returned for modification 4 August 2008/Accepted 10 October 2008

We studied the enrichment and distribution of the histone variant mH2A1 in the condensed inactive X (Xi) chromosome. By using highly specific antibodies against mH2A1 and stable HEK 293 cell lines expressing either green fluorescent protein (GFP)-mH2A1 or GFP-H2A, we found that the Xi chromosome contains ~1.5-fold more mH2A1 than the autosomes. To determine the in vivo distribution of mH2A1 along the X chromosome, we used a native chromatin immunoprecipitation-on-chip technique. DNA isolated from mH2A1-immunoprecipitated nucleosomes from either male or female mouse liver were hybridized to tiling microarrays covering 5 kb around most promoters or the entire X chromosome. The data show that mH2A1 is uniformly distributed across the entire Xi chromosome. Interestingly, a stronger mH2A1 enrichment along the pseudoautosomal X chromosome region was observed in both sexes. Our results indicate a potential role for macroH2A in large-scale chromosome structure and genome stability.

In the eukaryotic cell nucleus, DNA is packaged into chromatin. Chromatin exhibits a repetitive structure, and its basic unit, the nucleosome, consists of an octamer of core histones (two each of H2A, H2B, H3, and H4), around which two superhelical turns of DNA are wrapped (35).

In addition to the conventional core histones, cells express histone variants. Such histone variants are nonallelic forms of the conventional histones and are expressed in very small amounts within the cell. The histone variants display various degrees of similarity to their normal counterparts (34, 35). The most studied histone variants belong to the H2A and H3 families (7, 21, 30). When inserted into the histone octamer, variants may build nucleosomes with a different architecture and specialized functions (5, 7). For example, the crystal structure of the variant histone H2A.Z shows specific local molecular changes that could affect the stability of the H2A.Z nucleosome particle (32). This could explain, in turn, the reported distinct properties of H2A.Z nucleosomal arrays in solution (1, 15, 16, 32). Recent data demonstrated that a novel histone variant, H2A.Bbd, is less tightly bound both in vitro and in vivo in the nucleosome than is H2A (6, 17). The easier exchange and transfer of H2A.Bbd to an H3-H4 tetrameric particle could reflect the lower stability of the H2A.Bbd nucleosome compared to that of H2A (4, 17).

The histone variants play an important role in numerous vital cell processes as well as in several diseases (reviewed in references 7, 21, 30, and 37). For example, H2A.Z seems to be implicated in both the activation and repression of transcription (13, 20, 22, 31). The reported data suggested that H2A.Z is involved in chromosome segregation (29).

macroH2A (mH2A) is an unusual histone variant that consists of a domain similar to that of the conventional H2A (H2A-like domain) fused to a large nonhistone region (26). mH2A-reconstituted nucleosomes exhibit a modified structure with major alterations observed close to the dyad axis (3). These alterations interfere with the binding of the transcription factor NF-κB to its cognate sequence (3). In addition, SWI/SNF was unable to remodel and mobilize mH2A variant nucleosomes. In vitro experiments showed that the presence of mH2A repressed polymerase II transcription (14). It also has been reported that the presence of mH2A in the promoter results in the repression of transcription ex vivo (2, 25). In agreement with this, mH2A1 is depleted on active genes, and experiments with mH2A1$^{-/-}$ mice have shown that it is implicated in the silencing of endogenous murine leukemia viruses (9, 10).

Several reports using immunofluorescence approaches have claimed that the inactive X (Xi) chromosome is enriched with the histone variant mH2A (8, 11, 12, 23). However, the specificity of the association of mH2A with the Xi chromosome was challenged because, by using the same immunofluorescence approach combined with green fluorescent protein (GFP)-mH2A localization and fluorescent recovery after photobleaching analysis, it was shown that the enrichment of mH2A may reflect the higher chromatin concentration within the inactive highly condensed X chromosome (27).

In order to solve this disagreement in the literature, we have studied the distribution of mH2A on the Xi chromosome by using quantitative immunofluorescence and chromatin immunoprecipitation (ChIP)-on-chip techniques. We found that the Xi chromosome contains ~1.5-fold more mH2A1 than the

* Corresponding author. Mailing address: Institut Albert Bonniot, INSERM/UJF-U823, Site Santé-BP 170, 38042 Grenoble Cedex 9, France. Phone: (33) 4 76 54 94 73. Fax: (33) 4 76 54 95 95. E-mail: stefan.dimitrov@ujf-grenoble.fr.

▽ Published ahead of print on 20 October 2008.

autosomes. Intriguingly, mH2A1 shows uniform distribution all along the Xi chromosome.

MATERIALS AND METHODS

Cell culture and nucleus preparation. HEK 293 cells were grown in Dulbecco's modified Eagle's medium. Media were supplemented with 10% fetal bovine serum (Biowhittaker).

Immunofluorescence experiments. Cells grown on glass coverslips were fixed at 37°C in 4% paraformaldehyde, 2% sucrose and then permeabilized in phosphate-buffered saline (PBS) containing 0.2% Triton X-100 for 15 min. Free binding sites were blocked with 0.5 mg/ml bovine serum albumin, and specific antibodies were incubated for at least 30 min in PBS supplemented with 10% fetal bovine serum, 0.2% Tween 20, and 0.02% NaN_3. Unbound antibodies were removed by being washed with PBS, 0.2% Tween 20, and specific staining was revealed with Alexa 546-conjugated antibodies (Interchim, France). DNA was visualized with 4′,6′-diamidino-2-phenylindole (DAPI). Images were collected with a Zeiss 510 laser-scanning confocal apparatus with a ×40 oil-immersion objective. Stable cell lines expressing GFP-mH2A1.2 or GFP-H2A were generated using standard methods.

Mononucleosome and oligosome preparation. Nuclei were isolated from mouse livers. After the appropriate digestion of nuclei with micrococcal nuclease, linker histone-depleted chromatin (containing either mononucleosomes or oligosomes) was purified by centrifugation through sucrose gradients containing 0.6 M NaCl. The collected fractions then were dialyzed overnight against 50 mM NaCl, 1 mM EDTA, 10 mM Tris-HCl, pH 7.5, and, if necessary, concentrated on a Centricon device (optical density at 260 nm of 2 to 6).

mH2A1 ChIP. Immunoprecipitations were carried out as follows. The linker histone-depleted samples were incubated for 8 h at 4°C with immunopurified mH2A antibodies. Protein A-Sepharose beads were saturated with chicken erythrocyte nucleosomes (the anti-mH2A1 antibody we used does not recognize the chicken mH2A1) and then added to the mixture. The incubation lasted for 1 h under mild agitation at room temperature. Beads were washed five times in 50 mM NaCl, 1 mM EDTA, 10 mM Tris-HCl, pH 7.5, and finally recovered for protein or DNA extractions. Mononucleosomes represent the input, the first immunoprecipitation wash corresponds to the unbound fraction, and the beads contain the bound material. An amount of each fraction was loaded onto a gradient sodium dodecyl sulfate (SDS)–12 to 18% polyacrylamide gel electrophoresis and analyzed by Western blotting. Histones mH2A1 and H2A were detected successively on the same membrane. Nucleosomal DNA of each fraction was extracted from beads with a classical proteinase K digestion protocol.

Genome-wide mouse promoter DNA microarray hybridization. Genomic profiling was done by NimbleGen Systems as part of a ChIP array service. We used a mouse promoter tiling microarray set of two 385,000 arrays covering 5 kb (approximately positions −4000 to +1000) of 24,939 promoters, with a minimum spacing of 110 bp between probes (excluding repeated sequences). Probes were 45 to 85 nucleotides long and had an isothermal design (target melting point, 76°C). We provided nonamplified DNA from input and pull-down (5 μg each) samples to NimbleGen Systems for differential labeling by random priming using a Cy3/Cy5-coupled 9mer oligonucleotide and hybridization to oligonucleotide arrays. For each experiment, input and pull-down channel signal intensities and scaled $\log_2$ ratios were provided by NimbleGen Systems. For each probe, we divided the immunoprecipitated fraction/input fraction ratio from female liver chromatin by that from male liver chromatin, and we analyzed (by using *t* tests) the significance of the difference between the female/male ratio obtained with the X chromosome and that obtained with any autosome or the combination of all autosomes.

Hybridization on microarrays covering the whole mouse X chromosome. (i) Microarray design. Custom tiling microarrays were manufactured by NimbleGen Systems and were based on a probe selection provided by NimbleGen Systems. The probes were selected to be unique within the mouse genome at a median resolution of 306 bp across the entire X chromosome and at a median resolution of 227 bp for a part of chromosome 17 (4657287 to 19251247 in the NCBI m36 genome assembly). The microarray had 335,514 probes from chromosome X and 52,486 from chromosome 17. Note that repeated sequences were not present in the microarrays.

(ii) Hybridization. DNA was purified from mH2A-enriched chromatin and input chromatin. Labeling (red for ChIP samples, green for input samples), hybridization to microarrays, and data collection was performed by RZPD/ImaGenes.

(iii) Data analysis. Signals from chromosome 17 were used for normalization and scaling within and across microarrays on the assumption that mH2A distribution on chromosome 17 would be similar between males and females, unlike the case for the X chromosomes. Tukey's biweight function was determined from M values ($\log_2$ ChIP sample result/input sample result) from chromosome 17 signals of each array and subtracted from all M values for normalization. The mean absolute deviation of the M values across the normalized chromosome 17 signals in each array is used for scaling. A single-array-error model (19) was applied to calculate the confidence values, and a weighted average was used to combine replicas for males and females. In order to detect patterns within the data, the combined datasets were transformed using wavelet smoothening to generate continuous wavelet transform heat maps (33). Wavelet-smoothened data at the 64-kb scale was obtained using the maximal overlap discrete wavelet transform and was used for analyses (33).

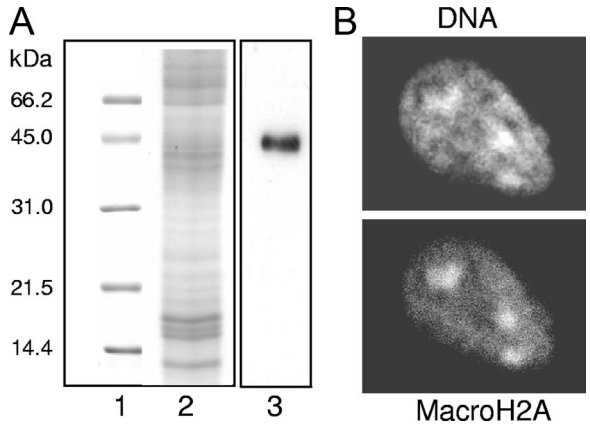

FIG. 1. Preferential staining of mH2A1 in the Xi chromosome of HEK 293 cells. (A) The anti-mH2A1 immunopurified antibody recognizes a single band with a molecular mass of ~42 kDa within an HEK 293 cell extract. The same amount of HEK 293 whole-cell extract was loaded on several wells of a 12% polyacrylamide gel containing SDS. After the completion of the electrophoresis, the gel was cut and one part of the gel was stained with Coomassie blue (lane 2), while the other part was used for Western blotting with anti-mH2A antibodies (lane 3). Lane 1, protein molecular mass marker. The same high specificity of the anti-mH2A1 antibody was observed when extract from mouse cells was used (not shown). (B) The mH2A1 antibody detects the Xi chromosome in HEK 293 cells at interphase. The top panel shows the nucleus of an HEK 293 cell stained with Hoechst, and the lower panel presents the immunostaining of the same cell with the mH2A1 antibody.

RESULTS

Quantitative immunofluorescence studies of the distribution of mH2A1. To study the association of mH2A with the Xi chromosome, we first developed a highly specific polyclonal antibody to mH2A1 (Fig. 1 to 3). The antibody was generated against the nonhistone region of mH2A1. In HEK 293 whole-cell extracts, the immunopurified antibody recognizes a single polypeptide with a molecular mass of 42 kDa, which corresponds to mH2A1 (Fig. 1A). We then used this antibody to study the distribution of mH2A1 in HEK 293 cells containing several Xi chromosomes. The immunofluorescence analysis demonstrated that the antibody preferentially stained several dense regions of the interphase HEK 293 cell nucleus, called Barr bodies, and corresponded to the Xi chromosome territories (Fig. 1B). These observations are in agreement with the reported immunofluorescence data (8, 11). However, an enhanced DAPI staining of the Xi chromosome also was observed (Fig. 1B and 2A). Since the enhanced DAPI staining is associated with a higher degree of compaction of the Xi chromosome even if mH2A1 is distributed uniformly over the nu-

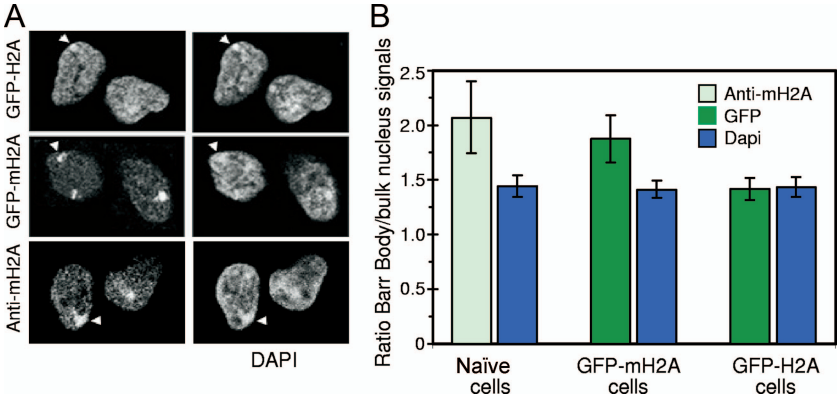

FIG. 2. Measurements of the amount of mH2A1 associated with the Xi chromosome in HEK 293 cells. HEK 293 cell lines stably expressing either GFP-H2A or GFP-mH2A1.2 and naïve HEK 293 cells were used to estimate the ratio of mH2A1 to H2A in the Xi chromosome and the autosomes. To visualize mH2A1 in the naïve cells, an immunopurified anti-mH2A1 antibody was used. (A) Preferential staining of the Xi chromosome with GFP-H2A, GFP-mH2A1, and anti-mH2A1 antibody (first row). The second row shows the DAPI staining of the nuclei. The arrow indicates the Xi chromosome. (B) The Xi chromosome is enriched in mH2A1. Images were deconvolved into two dimensions and then segmented with Metamorph software (Universal Imaging Corporation). The intensity of the fluorescence of the GFP and the anti-mH2A1 staining of the Xi chromosome in the three types of cells was measured. This also was done for a randomly chosen region of the nucleus with the same dimensions as those of the Xi chromosome, and the ratio between the fluorescence intensities of the two signals was calculated for the respective cells. The same ratio was calculated for the DAPI signals. Eighty GFP-mH2A1.2 or GFP-H2A cells and 20 naïve HEK 293 cells were used in the experiments. The bars indicate the standard deviations.

cleus, one would expect a higher signal intensity with the anti-mH2A1 antibody of the Xi chromosome, which would reflect the higher degree of compaction (i.e., the higher chromatin concentration) of the Xi chromosome (27). In agreement with this, in normal human female fibroblasts, all anti-conventional histone antibodies, as well as the anti-mH2A antibody, preferentially stained the Xi chromosome (27 and results not shown). Moreover, ectopically expressed GFP-mH2A and GFP-H2A were found concentrated on the Xi chromosome (27). Thus, the observed preferential staining might reflect an enrichment of mH2A1, a higher chromatin concentration, or both in the Xi chromosome.

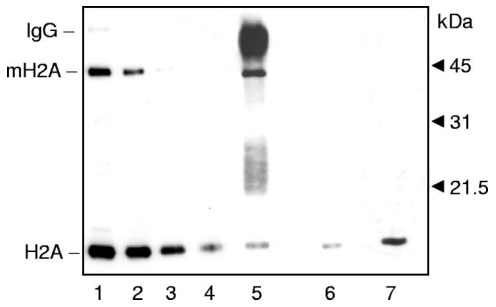

FIG. 3. ChIP of mH2A1 nucleosomes. Nuclei prepared from the liver of female mice were digested with micrococcal nuclease, and mononucleosomes were purified on a sucrose gradient containing 0.6 M NaCl to remove linker histones. Mononucleosomes were immunoprecipitated by using anti-mH2A antibodies attached to protein A agarose beads. Decreasing amounts of input nucleosomes (lanes 1 to 4; the nucleosome amount in each successive lane is decreased by twofold), the bound fractions (lane 5), and the unbound fractions (lane 6) were loaded on a 5 to 15% gradient polyacrylamide gel containing SDS. Lane 7 was loaded with control beads, which did not contain anti-mH2A antibodies but that were incubated with the nucleosomes. After the completion of the electrophoresis, the proteins were transferred to a nitrocellulose filter. The filter first was revealed with an mH2A antibody and then with an anti-H2A antibody. Note that mH2A gives a much stronger signal than H2A in the bound fraction (lane 5). In contrast, the mH2A signals of the input (lanes 1 to 4) and the unbound (lane 6) fractions are much less than the respective signals for H2A. IgG, immunoglobulin G.

To differentiate between these possibilities, we have carried out a quantitative analysis of the amount of mH2A1 associated with the Xi chromosome by using fluorescence microscopy and stable HEK 293 cell lines expressing either GFP-mH2A or GFP-H2A or naïve HEK 293 cells (Fig. 2A). Note that these cells commonly exhibit several Xi chromosomes (8). mH2A1 in the naïve cells was detected by using the anti-mH2A1 antibody (Fig. 2A). The intensity of the fluorescence signals of the GFP and the anti-mH2A1 staining for the three types of cells was measured. The same measurements were carried out for a randomly chosen region with the same dimensions as those of the Xi chromosome. The ratio of the two signals was calculated, and the same was done for the DAPI signals in the respective nuclei (Fig. 2B). The data clearly show that this ratio for the DAPI staining is close to 1.5 in the three types of cells (Fig. 2B). This demonstrates that in somatic cells the concentration of chromatin in the Xi chromosome is ~50% higher than that of autosomes. The ratio for the GFP fluorescence signals in the cells expressing GFP-H2A also was determined to be 1.5, which further confirms, as expected, the higher concentration of chromatin in the Xi chromosome and the accuracy of the DAPI measurements. The picture was different when we measured cells expressing GFP-mH2A1. The ratio of the mH2A fluorescence signals from the Xi chromosome compared to those autosomes in these cells was determined to be close to 2 (Fig. 2B). Similarly, the immunofluorescence staining of naive 293 cells with our mH2A antibody gave a nearly twofold-higher signal intensity for the Xi chromosome compared to that for the autosomes (Fig. 2B). Therefore, mH2A shows higher enrichment on the Xi chromosome than would be expected from the calculated chromatin concentration. We

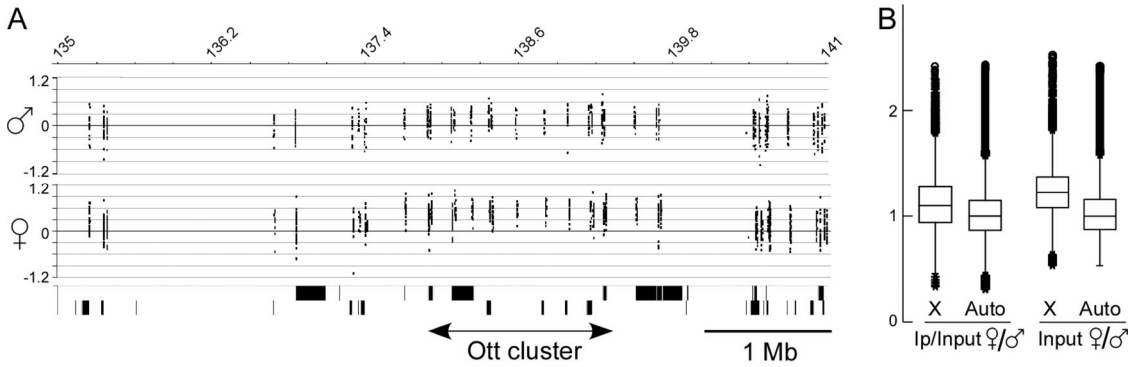

FIG. 4. mH2A1 enrichment on the promoters of the X chromosome of female and male mouse livers. Chromatin from both female and male mouse livers was immunoprecipitated with immunopurified anti-mH2A.1 antibody, and the input and bound DNA fractions were used without amplification for hybridization on tiling arrays containing probes covering 5 kb (about −4000 to +1000) of 24,939 mouse promoters. (A) Distribution of the $\log_2$ immunoprecipitated/input signal ratio of the promoter regions within a 6-Mb region encompassing the tandemly repeated Ott gene cluster. The top row shows genomic coordinates in megabase pairs (UCSC mm5 in NCBI build 33). The distribution of the signal that is generally centered around 0 is homogeneously shifted to higher values within the repeated region specifically in the female liver. (B) Comparative box plot analysis of the distribution of the mH2A enrichment levels in females and males on the different chromosomes. The ratios for both female and male bound (Ip)/input fractions and the female/male normalized input ratio are represented (indicated on the left and right, respectively). Data from all pooled autosomes (Auto) are compared to those from the X chromosome alone. Very similar distributions are observed when any individual autosome is analyzed.

conclude that the preferential staining of the Xi chromosome has two components: an enrichment of mH2A1 and a higher concentration of chromatin. Our data show that both components contribute to similar extents to the observed signal for the Xi chromosome.

Distribution of mH2A1 on the promoters reveals uniform enrichment on the X chromosome in the liver of female mice. Since mH2A1 might be involved in the repression of transcription, we first sought to detect whether enrichment on specific promoters could be detected. To test this, we carried out ChIP-on-chip experiments by using DNA tiling microarrays covering 5 kb around the transcription start site of 25,000 mouse promoters (NimbleGen Systems) and oligonucleosomes prepared from male or female mouse livers that were immunoprecipitated with anti-mH2A antibody. DNA from the input and immunoprecipitated (bound) fractions were isolated and used for hybridization. We immunoprecipitated sufficient material to avoid the amplification of the bound DNA, thus preventing biases due to PCR amplification.

Working with native nucleosomes preserves the mH2A1 epitopes and allows a very efficient ChIP (Fig. 3, compare lanes 5, 6, and 7). The enrichment of mH2A in the immunoprecipitated (bound) fraction can be directly estimated by SDS-gel electrophoresis and the Western blotting of input and bound proteins. Western blotting using the anti-mH2A1 antibody estimates the relative abundance of mH2A1 in the input and bound fractions (Fig. 3). Using the same blot but with an anti-H2A antibody (Fig. 3), the relative abundance of H2A in the input and bound fractions was estimated. The ratio between the mH2A1 and H2A signals is a measure of the enrichment of mH2A1 in the bound fraction. In the case of the bound fraction, this ratio is much greater than 1, while for the input fraction the ratio was less than 1 (Fig. 3, compare lane 5 to lanes 1 to 4). This analysis confirms that a very high enrichment of mH2A1 in the bound fraction was achieved. The mH2A1 and H2A signals of the Western blots of the input fractions (Fig. 3, lanes 1 to 4) were used to generate calibration curves to allow the calculation of the enrichment. In the different experiments, we found between 8- and 15-fold enrichment of mH2A1 in the bound fraction compared to that of the input material.

The analysis of the promoter tiling arrays after hybridization did not detect mH2A1 enrichment on specific promoters on female or male livers, except for a cluster of repeated genes belonging to the Ott family on the female livers (Fig. 4A). With most probes within this area, the ratio of immunoprecipitated fraction levels to input fraction levels was consistently higher in the female than in the male. The Ott family corresponds to a clustered X-specific intrachromosomal repeat, and most of the oligonucleotide probes within this region hybridized with a perfect match from 10 to 15 times to sequences repeated in close proximity on this portion of the X chromosome. As a consequence, the signal obtained with these probes was amplified, which could have allowed us to detect a weak and rather uniform mH2A1 enrichment that could have remained below detectable levels with the probes corresponding to the single-copy sequence. To detect such a weak enrichment, we compared the distribution of the signals obtained with all X chromosome probes to that of autosomal probes. When the immunoprecipitated/input ratio for each probe of the female liver chromatin is divided by that of the male liver chromatin, the distribution of these ratios between the X chromosome and other autosomes can be directly compared using a box plot representation (Fig. 4B). This comparison revealed that there was a weak but statistically highly significant mH2A1 enrichment ($P < 10^{-230}$ by t test) on the female X chromosome compared to that of the male one. This enrichment was observed when the X chromosome was compared to any autosomes or to all autosomes together, whereas the comparison of any autosome pair did not show such a difference (data not shown). Thus, our interpretation that the repeated Ott cluster allowed us to reveal a minor global enrichment of mH2A on the female X chromosomes appeared valid. Throughout the Ott cluster, we did not detect a higher enrichment at specific

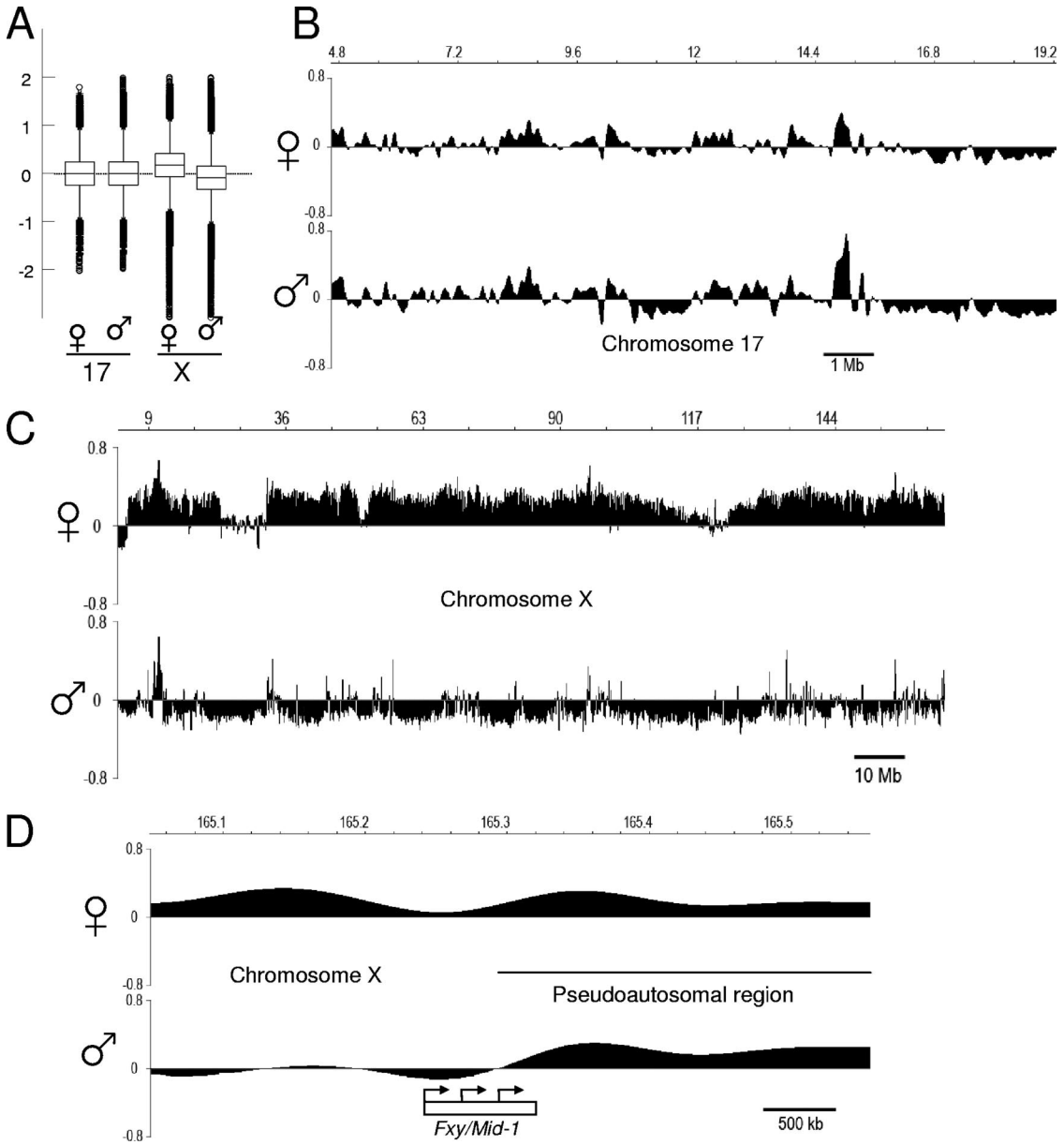

FIG. 5. mH2A1 enrichment on the whole length of the X chromosome of female and male mouse livers. Chromatin from both female and male mouse livers was immunoprecipitated with immunopurified anti-mH2A1 antibody, and the input and bound DNA (without PCR amplification) was used for hybridization on tiling arrays containing probes from the entire X chromosome and part of chromosome 17. M values ($\log_2$ immunoprecipitated signal/input signal) were normalized to chromosome 17 using a weighted average (Tukey's biweight function). Arrays were scaled using mean absolute deviations from chromosome 17 values. (A) Comparative box plot analysis of the distribution of the mH2A enrichment levels in the female and male on chromosomes 17 and X. (B to D) Wavelet analysis (33) was used to transform the combined ChIP-on-chip data sets to highlight broad patterns of mH2A1 association on the chromatin. Wavelet-smoothened data at the 64-kb scale was obtained using the maximal overlap discrete wavelet transform. The horizontal axes show genomic positions, while the vertical axes show the wavelet coefficient at that position at the 64-kb scale. The top row shows genomic coordinates (from the NCBI m36 genome assembly). (B) Chromosome 17 (4657287 to 19251247 in the NCBI m36 genome assembly). (C) X chromosome. mH2A1 enrichment is seen across the entire female X chromosome but not on the male X chromosome. The signal on the female X chromosome is the average of the contributions from both the active X and the Xi chromosomes. (D) A high degree of mH2A1 enrichment is seen in the PAR (28), starting from within the *Fxy*/*Mid-1* gene (depicted with a box; arrows show initiation sites of three annotated transcripts) of both the male and female X chromosomes.

positions relative to the transcription start site of the genes, suggesting that the mH2A enrichment at promoters is more global rather than specifically associated with promoter function.

Because the dynamic of the signal measured on microarrays always tends to be smaller than those in the initial nucleic acid population, we aimed at obtaining an estimation of the enrichment factor of mH2A1 on the female X chromosome by comparing the enrichment ratio detected for the female and male bound/input samples to that of the female input/male input

ratio normalized to the overall signal (Fig. 4B). Since the X/autosome ratio in the female is twice that in the male and the mH2A1 enrichment observed in the female is half the value observed for the normalized input, we estimate that there were about 1.5-fold higher levels of mH2A1 in the female X chromosome than in the male X chromosome. Assuming that the enrichment is due solely to the Xi chromosome in the female, we estimate that there is at most two times more mH2A1 on the Xi chromosome than on the active X chromosome.

Distribution of mH2A1 along the whole Xi chromosome. Because we did not detect enrichment on specific promoter regions, we next asked how mH2A1 is distributed along the Xi chromosome. We carried out a ChIP-on-chip experiment using DNA tiling microarrays covering the entire mouse X chromosome (Fig. 5). To be able to compare between different samples, particularly between males and female samples, we included 15% of the probes on the array from chromosome 17. Assuming that the mH2A1 distribution on chromosome 17 is similar or invariant between the sexes, we normalized and scaled the data within and between arrays using these chromosome 17 probes (Fig. 5). We observe a low-level but rather uniform chromosome-wide enrichment of mH2A1 on the female X chromosome, while the male X chromosome appears slightly depleted of mH2A1 relative to chromosome 17 (Fig. 5A, C). The low levels of enrichment may be in part because the female cell has an active as well as an inactive chromosome, and presumably the active X chromosome of females is slightly depleted of mH2A1, as it is in the single male X, thereby pulling down the average signal obtained from the Xi chromosome. Some regions of the female X chromosome do not show the enrichment (Fig. 5C). These regions correspond to rodent-specific regions that are not conserved in other mammals (http://genome.ucsc.edu/), suggesting that they have been acquired during evolution after the establishment of the mechanism allowing mH2A enrichment. Note that a relatively strong enrichment along the pseudoautosomal region (PAR) is observed for both sexes (Fig. 5D).

DISCUSSION

In this work, we have studied the origin of the higher staining of the Xi chromosome with anti-mH2A1 antibody and the distribution of mH2A1 along the whole length of the Xi chromosome by using quantitative fluorescence and ChIP-on-chip approaches. The GFP and immunofluorescence measurements show that the intensity of the mH2A1 staining of the Xi chromosome was approximately twice as strong as that of the autosomes. This was associated with the higher condensation of the Xi chromosome as well as with an enrichment of mH2A1 in the Xi chromosome, with both effects exhibiting very similar contributions; i.e., about 50% of the enhanced staining was due to the higher compaction of the Xi chromosome, and the remaining 50% reflected the preferential association of mH2A1 with the Xi chromosome. The ChIP-on-chip experiments demonstrated that a higher proportion of mH2A1 was associated with the X chromosomes in female than in male liver along the whole length of the X chromosomes, including promoters. This enrichment most likely was specific to the Xi chromosome based on the fluorescence analysis. Our quantitative analyses using these two types of approaches consistently revealed a 1.5- to 2-fold enrichment throughout the whole chromosome. Note that the antibody used showed a very low cross-reactivity (not exceeding 10 to 15%) with mH2A2 and, thus, the estimated larger amount of mH2A reflected only the enrichment of mH2A1 in the Xi chromosome.

Since the function of mH2A is not well understood, we can only hypothesize, at least for the moment, the meaning of our findings. mH2A appeared to be involved in transcriptional regulation. In vitro (14) and ex vivo (2) experiments pointed to an inhibitory role of mH2A in transcription. The depletion of mH2A1 in mice might regulate the expression of some genes (9) and appeared to be important for the silencing of endogenous murine leukemia viruses (10). However, the stable chromosome X inactivation requires mH2A1 (18). Since no specific enrichment of mH2A1 on the promoter regions of the Xi chromosome genes was observed, the potential role of mH2A1 in Xi chromosome silencing should not involve a positioned nucleosome on the promoters, as was the case for B cells (2). Instead, we speculate that an mH2A1-dependent chromatin structure above the nucleosomal level is involved in the X chromosome inactivation. The number of nucleosomes containing mH2A was estimated to be around 3% of the total number of nucleosomes, and bearing in mind the enrichment of mH2A1 on the Xi chromosome (according to the data presented in this work), close to 4 to 6% of the Xi chromosome nucleosomes should contain mH2A1. Thus, each 15th to 25th Xi chromosome nucleosome is an mH2A nucleosome. These mH2A nucleosomes, which are uniformly distributed on the Xi chromosome, could interact with some other factors and form some coating around the Xi chromosome and assist in its compaction and the maintenance of its inactive state. A potential candidate is PARP-1. Indeed, PARP-1 was found to be associated with mH2A nucleosomes in vivo (24, 25), and it was shown that the association of PARP-1 promotes its condensation in vitro (36).

Of note, we have measured an enrichment of mH2A1 on the PAR of both inactive and active chromosome X. This enrichment was higher than the bulk enrichment of mH2A1 on the Xi chromosome. The PAR is the region where the X and Y chromosomes are homologous, and the homologous pairing of the XY body takes place during meiosis. This suggests that mH2A1 is implicated in homologous recombination during meiosis. The assumption is that the small PAR of mice needs to generate one crossover per meiosis and, thus, has been selected for high recombination efficiency. Consequently, mH2A could be part of the machinery to silence these hyperrecombinogenic sequences to ensure genome stability in the soma. We predict that apart from being involved in gene regulation, mH2A is involved in suppressing chromosome recombination and serves a function in genomic stability.

ACKNOWLEDGMENTS

This work was supported by INSERM, CNRS, and ANR project no. NT05-1_41978 and by the GEN-AU initiative of the Austrian Ministry of Science.

S.D. acknowledges La Ligue Nationale contre le Cancer (Equipe labelisée La Ligue). We thank H. Fiegler and N. P. Carter for help in the initial stage of this work.

REFERENCES

1. **Abbott, D. W., V. S. Ivanova, X. Wang, W. M. Bonner, and J. Ausio.** 2001. Characterization of the stability and folding of H2A.Z chromatin particles: implications for transcriptional activation. J. Biol. Chem. **276:**41945–41949.
2. **Agelopoulos, M., and D. Thanos.** 2006. Epigenetic determination of a cell-specific gene expression program by ATF-2 and the histone variant macroH2A. EMBO J. **25:**4843–4853.
3. **Angelov, D., A. Molla, P. Y. Perche, F. Hans, J. Cote, S. Khochbin, P. Bouvet, and S. Dimitrov.** 2003. The histone variant MacroH2A interferes with transcription factor binding and SWI/SNF nucleosome remodeling. Mol. Cell **11:**1033–1041.
4. **Angelov, D., A. Verdel, W. An, V. Bondarenko, F. Hans, C. M. Doyen, V. M. Studitsky, A. Hamiche, R. G. Roeder, P. Bouvet, and S. Dimitrov.** 2004. SWI/SNF remodeling and p300-dependent transcription of histone variant H2ABbd nucleosomal arrays. EMBO J. **23:**3815–3824.
5. **Ausió, J., and D. W. Abbott.** 2002. The many tales of a tail: carboxyl-terminal tail heterogeneity specializes histone H2A variants for defined chromatin function. Biochemistry **41:**5945–5949.
6. **Bao, Y., K. Konesky, Y. J. Park, S. Rosu, P. N. Dyer, D. Rangasamy, D. J. Tremethick, P. J. Laybourn, and K. Luger.** 2004. Nucleosomes containing the histone variant H2A.Bbd organize only 118 base pairs of DNA. EMBO J. **23:**3314–3324.
7. **Boulard, M., P. Bouvet, T. K. Kundu, and S. Dimitrov.** 2007. Histone variant nucleosomes: structure, function and implication in disease. Subcell. Biochem. **41:**71–89.
8. **Chadwick, B. P., and H. F. Willard.** 2001. Histone H2A variants and the inactive X chromosome: identification of a second macroH2A variant. Hum. Mol. Genet. **10:**1101–1113.
9. **Changolkar, L. N., and J. R. Pehrson.** 2006. macroH2A1 histone variants are depleted on active genes but concentrated on the inactive X chromosome. Mol. Cell. Biol. **26:**4410–4420.
10. **Changolkar, L. N., G. Singh, and J. R. Pehrson.** 2008. macroH2A1-dependent silencing of endogenous murine leukemia viruses. Mol. Cell. Biol. **28:**2059–2065.
11. **Costanzi, C., and J. R. Pehrson.** 1998. Histone macroH2A1 is concentrated in the inactive X chromosome of female mammals. Nature **393:**599–601.
12. **Costanzi, C., and J. R. Pehrson.** 2001. macroH2A2, a new member of the macroH2A core histone family. J. Biol. Chem. **276:**21776–21784.
13. **Dhillon, N., and R. T. Kamakaka.** 2000. A histone variant, Htz1p, and a Sir1p-like protein, Esc2p, mediate silencing at HMR. Mol. Cell **6:**769–780.
14. **Doyen, C. M., W. An, D. Angelov, V. Bondarenko, F. Mietton, V. M. Studitsky, A. Hamiche, R. G. Roeder, P. Bouvet, and S. Dimitrov.** 2006. Mechanism of polymerase II transcription repression by the histone variant macroH2A. Mol. Cell. Biol. **26:**1156–1164.
15. **Fan, J. Y., F. Gordon, K. Luger, J. C. Hansen, and D. J. Tremethick.** 2002. The essential histone variant H2A.Z regulates the equilibrium between different chromatin conformational states. Nat. Struct. Biol. **9:**172–176.
16. **Fan, J. Y., D. Rangasamy, K. Luger, and D. J. Tremethick.** 2004. H2A.Z alters the nucleosome surface to promote HP1alpha-mediated chromatin fiber folding. Mol. Cell **16:**655–661.
17. **Gautier, T., D. W. Abbott, A. Molla, A. Verdel, J. Ausio, and S. Dimitrov.** 2004. Histone variant H2ABbd confers lower stability to the nucleosome. EMBO Rep. **5:**715–720.
18. **Hernández-Muñoz, I., A. H. Lund, P. van der Stoop, E. Boutsma, I. Muijrers, E. Verhoeven, D. A. Nusinow, B. Panning, Y. Marahrens, and M. van Lohuizen.** 2005. From the cover: stable X chromosome inactivation involves the PRC1 polycomb complex and requires histone MACROH2A1 and the CULLIN3/SPOP ubiquitin E3 ligase. Proc. Natl. Acad. Sci. USA **102:**7635–7640.
19. **Hughes, T. R., C. J. Roberts, H. Dai, A. R. Jones, M. R. Meyer, D. Slade, J. Burchard, S. Dow, T. R. Ward, M. J. Kidd, S. H. Friend, and M. J. Marton.** 2000. Widespread aneuploidy revealed by DNA microarray expression profiling. Nat. Genet. **25:**333–337.
20. **Larochelle, M., and L. Gaudreau.** 2003. H2A.Z has a function reminiscent of an activator required for preferential binding to intergenic DNA. EMBO J. **22:**4512–4522.
21. **Malik, H. S., and S. Henikoff.** 2003. Phylogenomics of the nucleosome. Nat. Struct. Biol. **10:**882–891.
22. **Meneghini, M. D., M. Wu, and H. D. Madhani.** 2003. Conserved histone variant H2A.Z protects euchromatin from the ectopic spread of silent heterochromatin. Cell **112:**725–736.
23. **Mermoud, J. E., C. Costanzi, J. R. Pehrson, and N. Brockdorff.** 1999. Histone macroH2A1.2 relocates to the inactive X chromosome after initiation and propagation of X-inactivation. J. Cell Biol. **147:**1399–1408.
24. **Nusinow, D. A., I. Hernandez-Munoz, T. G. Fazzio, G. M. Shah, W. L. Kraus, and B. Panning.** 2007. Poly(ADP-ribose) polymerase 1 is inhibited by a histone H2A variant, macroH2A, and contributes to silencing of the inactive X chromosome. J. Biol. Chem. **282:**12851–12859.
25. **Ouararhni, K., R. Hadj-Slimane, S. Ait-Si-Ali, P. Robin, F. Mietton, A. Harel-Bellan, S. Dimitrov, and A. Hamiche.** 2006. The histone variant mH2A1.1 interferes with transcription by down-regulating PARP-1 enzymatic activity. Genes Dev. **20:**3324–3336.
26. **Pehrson, J. R., and V. A. Fried.** 1992. MacroH2A, a core histone containing a large nonhistone region. Science **257:**1398–1400.
27. **Perche, P., C. Vourch, C. Souchier, M. Robert-Nicoud, S. Dimitrov, and C. Khochbin.** 2000. Higher concentrations of histone macroH2A in the Barr body are correlated with higher nucleosome density. Curr. Biol. **10:**1531–1534.
28. **Perry, J., S. Palmer, A. Gabriel, and A. Ashworth.** 2001. A short pseudoautosomal region in laboratory mice. Genome Res. **11:**1826–1832.
29. **Rangasamy, D., I. Greaves, and D. J. Tremethick.** 2004. RNA interference demonstrates a novel role for H2A. Z in chromosome segregation. Nat. Struct. Mol. Biol. **11:**650–655.
30. **Redon, C., D. Pilch, E. Rogakou, O. Sedelnikova, K. Newrock, and W. Bonner.** 2002. Histone H2A variants H2AX and H2AZ. Curr. Opin. Genet. Dev. **12:**162–169.
31. **Santisteban, M. S., T. Kalashnikova, and M. M. Smith.** 2000. Histone H2A.Z regulates transcription and is partially redundant with nucleosome remodeling complexes. Cell **103:**411–422.
32. **Suto, R. K., M. J. Clarkson, D. J. Tremethick, and K. Luger.** 2000. Crystal structure of a nucleosome core particle containing the variant histone H2A.Z. Nat. Struct. Biol. **7:**1121–1124.
33. **Thurman, R. E., N. Day, W. S. Noble, and J. A. Stamatoyannopoulos.** 2007. Identification of higher-order functional domains in the human ENCODE regions. Genome Res. **17:**917–927.
34. **Tsanev, R., G. Russev, I. Pashev, and J. Zlatanova.** 1993. Replication and transcription of chromatin. CRC Press, Boca Raton, FL.
35. **van Holde, K.** 1988. Chromatin. Springer-Verlag KG, Berlin, Germany.
36. **Wacker, D. A., D. D. Ruhl, E. H. Balagamwala, K. M. Hope, T. Zhang, and W. L. Kraus.** 2007. The DNA binding and catalytic domains of poly(ADP-ribose) polymerase 1 cooperate in the regulation of chromatin structure and transcription. Mol. Cell. Biol. **27:**7475–7485.
37. **Zlatanova, J., and A. Thakar.** 2008. H2A.Z: view from the top. Structure **16:**166–179.